Materials Transactions, Vol. 58, No. 3 (2017) pp. 341 to 349
Special Issue on New Proposals on Titanium Production and Molten Salts

Reduction of $CaTiO_3$ in Molten $CaCl_2$ - as Basic Understanding of Electrolysis

Ryosuke O. Suzuki[*1], Hiromi Noguchi, Hiromasa Hada[*2], Shungo Natsui and Tatsuya Kikuchi

Faculty of Engineering, Hokkaido University, Sapporo 060–8628, Japan

Electrochemical decomposition of $CaTiO_3$ at the cathode was examined in a scheme of titanium metal production from natural deposit, Ilmenite ($TiFeO_3$). Based on the possible precipitation of $CaTiO_3$ from $TiFeO_3$, the electrochemical decomposition of $CaTiO_3$ is here examined using combination of the calciothermic reduction and the electrolysis of CaO in the same molten salt. Inhomogeneous reduction in the cathodic basket is related with buoyancy of Ca and insufficient dehydration. By optimizing the cooling conditions, CaO content in the molten salt, and dehydration method, an industrial level of 0.42 mass%O could be achieved as powder form. [doi:10.2320/matertrans.MK201625]

(Received September 5, 2016; Accepted October 17, 2016; Published December 2, 2016)

Keywords: *calcium chloride, calciothermic reduction, molten salt electrolysis, titanium production*

1. Introduction

1.1 Oxide reduction in the chloride melt

Electrochemical decomposition of oxides at the cathode has been examined by using $CaCl_2$-CaO or LiCl-Li_2O molten salts. Fray, Chen and coworkers[1–4] have extensively studied the reduction of TiO_2, and they proposed "FFC Cambridge Process" that the oxide anion from the solid oxide pellet placed at the cathode transfers to the anode in the salt bath. Because Ti-O binary system contains many lower oxides than TiO_2[5], oxygen in a higher oxide is removed to form a lower oxide. Namely, by receiving the electric charge from the cathode, the oxide MeO_{x+1} is ionized as,

$$MeO_{x+1}(s) + 2e^- = MeO_x(s) + O^{2-} \quad (1)$$

When the lowest oxide MeO_x can be also ionized, it is possible to obtain the metal (Me) at the cathode by repeating the ionization of a series of oxides as shown in eq. (1). However, the decomposition voltage increases as the valence of Me decreases. By applying the voltage larger than 2.4 V[6] (the decomposition potential of pure CaO to pure oxygen gas) above the melting temperature of $CaCl_2$, CaO in $CaCl_2$ melt is decomposed to metallic Ca and the oxide anion[7–9].

$$CaO = Ca^{2+} + O^{2-} \quad (2)$$

$$Ca^{2+} + 2e^- = Ca \text{ (at cathode)} \quad (3)$$

$$2O^{2-} = O_2(g) + 4e^- \text{ (at anode)} \quad (4)$$

Because CaO can dissolve in molten ionic $CaCl_2$ as large as 20 mol%CaO[10–12], it is natural that CaO is ionized as eq. (2) and thermochemical activity of CaO should be less than 1. Pure oxygen gas will be adhered on the surface of anode, although it is not easy to allow oxygen gas evolution. The severe anodic oxidation causes dissolution of metallic anode. Carbon is most commonly chosen as one of stable materials for anode in $CaCl_2$ melt. In case of carbon anode, O^{2-} preferentially reacts with C to form CO and/or CO_2 gas on the surface as[7–9],

$$C + O^{2-} = CO(g) + 2e \quad (5)$$

$$C + 2O^{2-} = CO_2(g) + 4e \quad (6)$$

The decomposition voltage for CO/CO_2 gas formation becomes about 1.0 V lower than that for O_2 gas evolution[6]. This is because pure O_2 gas evolution was rarely found.

1.2 Reduction by Calcium

The deposited Ca at the cathode in eq. (3) dissolves in the $CaCl_2$ melt, because the solubility of Ca is reported as about 4 mol%Ca[13–18]. The droplets of Ca may be found as the "metal fog" near the cathode[19,20], when Ca dissolution rate is delayed. This Ca-rich environment can be considered as a powerful reductant, even if it does not hold the highest chemical reactivity such as pure Ca. In the mechanism of "OS process", the calciothermic reduction accompanied with this dissolved Ca at the vicinity of the cathode is essential, where the oxide is placed close to the cathode[9,21–24].

$$MeO_{x+1}(s) + Ca \text{ (in } CaCl_2) = MeO_x(s) + CaO \quad (7)$$

The dissolved calcium works effectively to reduce the oxide powder, even if these particles do not have any direct electronic contact with the cathode, or even if the oxides are electronically insulators, or even if their state are gas or liquid. The contribution of electric conduction in OS process[9,21–24] are different from that of the FFC-Cambridge process[1–4].

The by-product CaO in eq. (7) should decompose as shown by eqs. (2)–(4), or form CO and CO_2 gas as shown by eq. (5) and eq. (6), respectively. However, the excess amount of CaO may form the Ca-containing complex oxide with the residual oxide, such as $CaTiO_3$ and Ca_2TiO_4 as the intermediate products[23–25]. Note that Ca_2TiO_4 contains trivalent Ti and it can be grown only in $CaCl_2$ melt with metallic Ti[26]. The appearance of these Ca-containing complex oxides in the way of reduction is one of the proofs that the calciothermic reduction (OS process) is working. A small addition of CaO in $CaCl_2$ improved the rate of reduction and deoxidation[23]. However, CaO in the salt can react with TiO_2 to form $CaTiO_3$ without any apparent electron transfer. This is also evidence that the calciothermic reduction occurs in the molten salt. Calcium deoxidation in pure Ti could achieve a very low oxygen level less than 100 mass ppmO[27,28], although the commercial pure

[*1]Corresponding author, E-mail: rsuzuki@eng.hokudai.ac.jp
[*2]Graduate Student, Hokkaido University. Present address: Nagoya works, Nippon Steel & Sumitomo Metal Co. Ltd., Tokai 476–8686, Japan

titanium is contaminated as high as a few thousands ppm.

1.3 Reduction of TiO_2 in CaO-$CaCl_2$ melt

The ternary phase equilibrium of Ca-Ti-O system at 1273 K was reported[29], but it contained some discrepancy with various experimental conditions[29,30]. As shown in Fig. 1[30], no phase exits inside of the small triangle of Ca-CaO-Ti. Although some phases stably exist in the quasi-binary phase diagram of TiO_2 and CaO[31–33], no other phases were experimentally reported except for $CaTiO_3$, when they coexist with $CaCl_2$ melt. Using the phase diagram equilibrated with $CaCl_2$ melt[30], the route of the phase transition from TiO_2 to the metallic Ti is predicted as follows.

When TiO_2 was taken as the starting material for reduction, the averaged concentration in the reactor stays on a conjugation tie line between TiO_2 and Ca, as indicated in Fig. 1. Therefore, the precipitation of $CaTi_2O_4$ from TiO_2 should be found as the intermediate phase from the view of local thermodynamic equilibrium[24]. After rapid decomposition of $CaTi_2O_4$, three-phase phase equilibrium among $CaTiO_3$, $CaTi_2O_4$ and α-Ti (at Ti_2O composition) will be realized. The next three-phase equilibrium among $CaTiO_3$, α-Ti and CaO shows the disproportional reaction from $CaTi_2O_4$ (valency of Ti: +3) to $CaTiO_3$ (+4) and α-Ti (0). Because of dissolution of the byproduct CaO in $CaCl_2$ melt, the three-phase equilibrium among $CaTiO_3$, α-Ti and CaO successively shifts to a new two-phase equilibrium of CaO and α-Ti, to three-phase equilibrium among α-Ti, β-Ti and CaO, and finally to two-phase equilibrium of CaO and β-Ti.

In representation as chemical equation, this sequence can be written as,

$$\begin{aligned} TiO_2 &\rightarrow CaTi_2O_4 \rightarrow (CaTiO_3,\ CaTi_2O_4 \text{ and } \alpha\text{-Ti}) \\ &\rightarrow (CaTiO_3,\ \alpha\text{-Ti and CaO}) \rightarrow (\alpha\text{-Ti and CaO}) \\ &\rightarrow (\alpha\text{-Ti},\ \beta\text{-Ti and CaO}) \rightarrow (\beta\text{-Ti and CaO}) \end{aligned} \quad (8)$$

The first reaction (from TiO_2 to $CaTi_2O_4$) was not common in the experiments[24], however, the existence of $CaTi_2O_4$ was confirmed at the central part of oxide pellet by *in-situ* X-ray diffraction[25]. Because the stability of $CaTi_2O_4$ is weak, it is thought that the single phase could not be practically formed. The existence of $CaTiO_3$ as intermediate phase has been well reported in the previous studies[1–4,8,9,21–23,25], however, its meta-stable existence is considered as a barrier to obtain pure β-Ti in the route from TiO_2 to Ti[23–25,30,34]. The final phase transition is known as "deoxidation from α-Ti"[27,28]. The obtained pure β-Ti transform to α-Ti during cooling to room temperature[5].

Therefore, looking for the best conditions to achieve the lowest oxygen content in the ever-obtained Ti powders, the decomposition of $CaTiO_3$ and the successive oxygen removal from α-Ti and β-Ti are key points. Too quick decomposition of $CaTiO_3$ causes the particles coarsening of metal Ti so that the deoxidation from α-Ti particles becomes slower. On the other hand, the slow decomposition of $CaTiO_3$ causes CaO trap among the Ti particles[30,34]. Once CaO was caught at the grain boundary, it is difficult to dissolve CaO in the wet chemical procedure. Therefore, the detailed reduction behavior of $CaTiO_3$ is worth to be clarified experimentally[30,34]. The effective decomposition of $CaTiO_3$ in $CaCl_2$ melt is important to obtain high quality of Ti when the starting material is TiO_2. Ca in $CaTiO_3$ is rigidly hold in the crystalline structure of oxide, however, once $CaTiO_3$ is reduced to Ti, Ca in $CaTiO_3$ may contribute as a suitable reductant during the electrolysis. Because it is reported that the reduction of $CaTiO_3$ is faster than that of TiO_2 at the initial range of reduction[30], the reduction of $CaTiO_3$ may realize the cost-affordable titanium production through $CaTiO_3$ from the oxide ores.

1.4 Reduction of $CaTiO_3$ in CaO-$CaCl_2$ melt

Due to depletion of high quality of TiO_2 ore, ilmenite ore (mainly $TiFeO_3$) has been used for TiO_2 production, which is also served to Kroll process for Ti metal production, as shown in Fig. 2. TiO_2 was originally considered as the starting material for OS process[7–9], but some trials on $TiFeO_3$ reduction have been reported to produce Ti-Fe alloy[35–37]. However the iron removal is needed as the major impurity for usage as pure Ti, because Ti metal becomes brittle by a small addition of Fe. Once the sponge titanium is polluted by Fe in Kroll process, it was difficult to remove Fe.

Fe should be practically separated at the earlier stage of

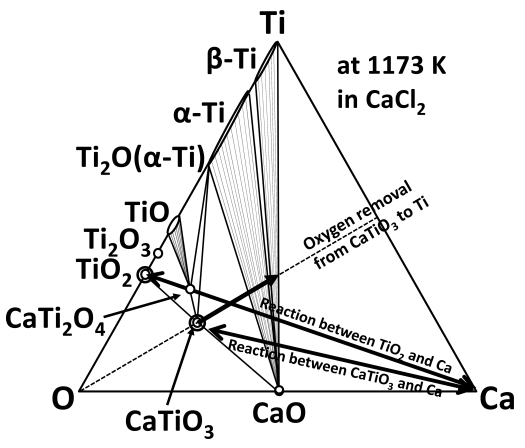

Fig. 1 Phase equilibria in Ca-Ti-O system coexisted with $CaCl_2$ melt[30]. Reduction route from $CaTiO_3$ to metallic Ti is inserted when oxygen is removed as CaO.

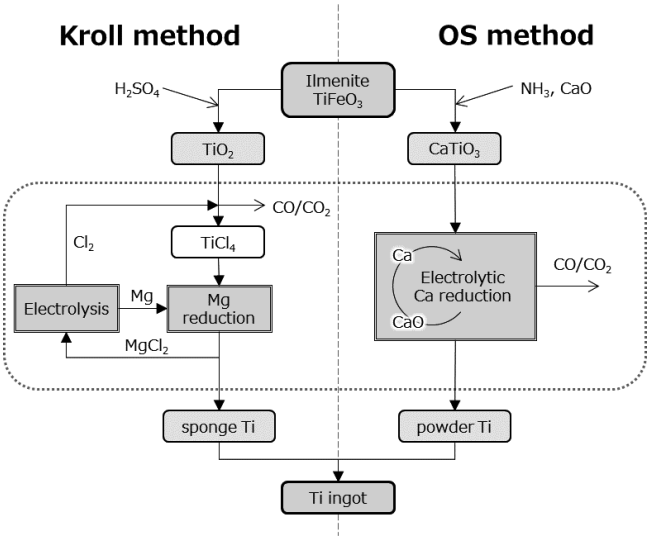

Fig. 2 Flowsheet of designed procedure starting from Ilmenite to Ti ingot via $CaTiO_3$ in comparison with Kroll process.

processing such as at oxide formation. Fe removal is also needed for oxide reduction techniques such as FFC Cambridge and OS processes. If we are allowed to take $CaTiO_3$ as the intermediate material for Ti metal production, and if we can remove Fe component on the way from $TiFeO_3$ to $CaTiO_3$ as shown in Fig. 2, we can skip at least one process to form TiO_2.

The purpose of this paper is to show the fundamental optimization in electrochemical reduction of $CaTiO_3$ in the molten CaO-$CaCl_2$. The authors will report the results on a new route from $TiFeO_3$ to $CaTiO_3$ precisely in a separate paper. As the $CaTiO_3$ particles suitable for OS process could be obtained, this paper reports the efficient operating conditions to form Ti metal from $CaTiO_3$ and to remove oxygen in Ti in the framework of OS process. The goal concerning the quality of Ti will be set as the same level of commercially available Ti, such as a few thousands mass ppm oxygen. The authors believe that this basic analysis will be helpful to produce a high quality of Ti not only from $CaTiO_3$ but also in reduction of TiO_2.

2. Experimental

Anhydrous $CaCl_2$ was heated at 573 K for a few days in air for dehydration. 600 g of $CaCl_2$ was mixed with a small amount of CaO that had been calcined at 1373 K in air to decompose the possible contamination of $CaCO_3$. The mixture was filled in dense MgO crucible (90 mm inside diameter, 200 mm depth), and heated in vacuum. Ar gas was introduced prior to electrolysis at 1173 K. The anode and cathode consisted of carbon bar (10 mm in diameter) and metallic basket (Ti or stainless steel (SUS316L) net of #100), respectively, and they were connected to the stainless bar and Ti bar, respectively, as the current leads. A constant voltage of 3.0 V was applied between these two bars. The oxide powder was filled in the cathodic basket before heating, and the electrodes were inserted after melting of the salt. Current, voltage, pressure and temperature were measured and recorded in 10 s interval.

The obtained powder was washed by drinking water, a dilute acetic acid, distilled water, ethanol and acetone, in this order. It was kept in vacuum before analyses. The phases were identified by X-ray diffraction (XRD) measurement. The oxygen content and particle size distribution were analyzed by LECO TC-600 oxygen analyzers and Microtrac MT3000II, respectively. The particle surface was observed by scanning electron microscopy (SEM, Hitachi TM-1000).

High purity $CaTiO_3$ powder for this work was purchased from four producers, Alfa Aesar, Furuuchi Chemical Corporation, Kojundo Chemical Laboratory Corporation and Soekawa Rikagaku Corporation. They are hereafter denoted as #A, #F, #K and #S, respectively.

3. Results and Discussion

3.1 Oxygen distribution in the cathodic basket

2.0 g of $CaTiO_3$ powder (particle size <20 μm) was filled in cathodic basket. After dehydration at 1173 K, Ar gas was filled in the vessel, and the electrolysis was conducted in Ar gas flowing at 1173 K. After the electrolysis for a period between several hours to a day, the cathode was pulled up from the molten salt, and cooled in Ar gas atmosphere in the rate of $1/60$ Ks^{-1}. The residual oxygen was analyzed at several positions from the cathode.

Figure 3 shows the cross-sectional view of basket in which the oxide powder was filled. The diameter of Ti bar was set 6.0 mm, and the diameter of Ti disk at the bottom of basket determined the diameter of cathodic basket. Depending on the diameter of the basket between 9–30 mm, the packed depth of oxide powder was varied between 20–4 mm, respectively, when the basket was recovered from the molten salt. The reduced sample was roughly separated in 4 parts; the inner and outer parts at the upper and lower position. As shown in Fig. 3, they were denoted as #1 to #4.

The supplied electricity Q during the electrolysis was evaluated by integrating the current during time. Q is normalized by Q_0, where Q_0 is the stoichiometric charge to form Ca equivalent to reduce the charged amount of $CaTiO_3$ by assuming the apparent reaction as,

$$CaTiO_3 + 2\underline{Ca} = 3CaO + Ti \quad (9)$$

$$Ca^{2+} + 2e = \underline{Ca} \quad (10)$$

Therefore, $Q/Q_0 = 100\%$ is an index of electric charge to reduce all the charged oxide in an ideal condition of eqs. (9) and (10).

Figure 4 shows the residual oxygen in the obtained powder at these 4 portions after the electrolysis of $Q/Q_0 = 200\%$. The upper parts were fairly well reduced to the level of 7 mass%O, while the lower parts contained a higher level of oxygen. The phases existing in the sampling portion were identified by XRD measurement such as Ti_3O and Ti_2O. They were α-Ti at the operating temperature, and decomposed during cooling. They corresponded to the oxygen level.

The outer parts of the basket were better deoxidized to the

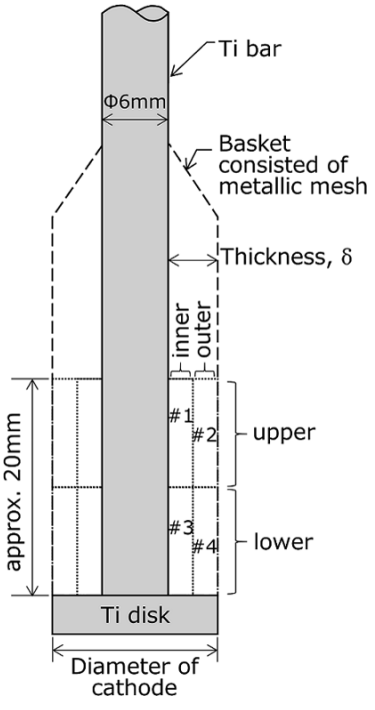

Fig. 3 cross-sectional view of the cathodic basket.

lower level. Note that the stainless steel (SUS316L) net was used as the basket material. It neither reacts with the oxide nor removes oxygen, although mutual diffusion of metallic elements occurred for a few days operation. In case of Ti basket, there remained the possibility of reaction between the oxide and Ti net.

The difference of oxygen level by height in the powder may be caused by the density difference. The densities of $CaCl_2$ and Ca are 2.0 Mg/m^3 and 1.37 Mg/m^3, respectively. The lighter Ca floats at the upper portion of heavier molten $CaCl_2$. Because Ca metal deposits preferentially on the cathodic surface such as on the metallic net, Ca droplets or highly Ca-dissolved liquid flows upward along the outer surface of basket, as illustrated in Fig. 5. Although the current concentrates to the edges of cathode such as Ti disk at the bottom, the precipitate does not remain there and begins to flow upward.

It is not easy to explain this oxygen distribution in the framework of FFC mechanism, because the larger current density at the lower portion seems to cause the better deoxidization due to edge effect in electrolysis. The oxygen distribution in the packed powder may be characteristic as calciothermic reduction in the molten salt. Therefore, the upward flow of Ca-containing salt close to the oxide sample should be regulated for the effective reaction with the oxide.

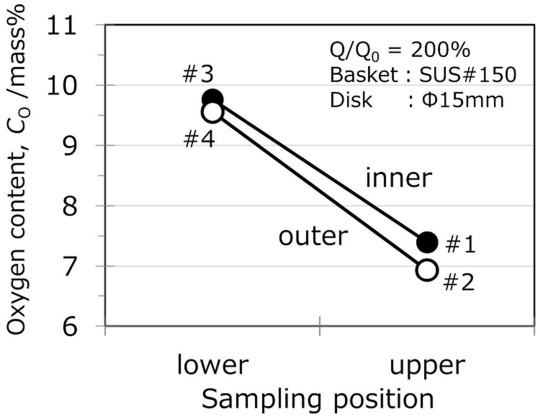

Fig. 4 Oxygen contents in the sample reduced at $Q/Q_0 = 200\%$.

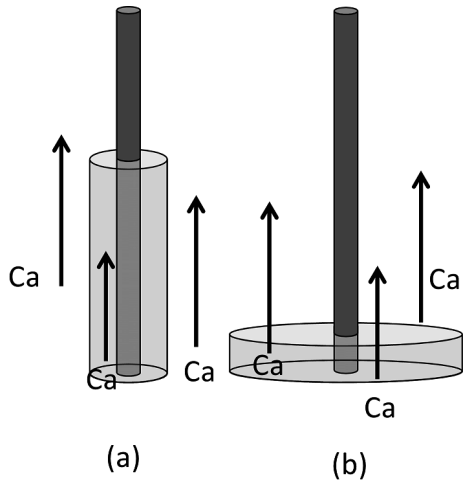

Fig. 5 illustration of reaction model of deposited Ca and the oxide. (a) slim basket and (b) thick basket.

3.2 Reduction in various baskets

The exposed time of oxide to Ca is limited at the lower portion as illustrated in Fig. 5(a), while it is longer at the upper part as in Fig. 5(a). The exposed time at the slim basket (Fig. 5(a)) is longer than that of the thicker basket (Fig. 5(b)), because the same amount of oxides were filled. The physical contact between Ca or Ca-dissolved liquid and the oxide powder will affect the degree of oxygen level.

Figure 6 shows the residual oxygen when the diameter of cathodic basket was varied. The oxygen concentration was averaged over 4 portions; the sample after electrolysis was not separated by the location. The whole sample was mixed well for analysis.

The same amount of oxide (2.0 g) was filled in the basket, and the same amount of electricity was supplied (Q/Q_0 = 200%). The thickness of the sample is defined as illustrated in Fig. 3. When the thickness becomes smaller, the oxygen level even at the inner part could be decreased.

The mesh spacing (#100–#200) and stitch (plain or twill weave) did not significantly affect the oxygen concentration in the reduced sample. This means that the Ca deposit can invade into the central part of oxide without any severe disturbance of mesh opening or particle spacing (a few tens μm). Namely the pore among the metallic particles such as a few tens μm does not affect the adhesion and wettability of reductant, Ca, or Ca-containing salt.

When Ti mesh was used as shown in Fig. 6, the oxygen level slightly decreased because Ti has so strong affinity with oxygen that Ti may absorb oxygen in the oxide. Ti mesh with opening of #100 was hereafter taken as the standard material for cathodic basket. The thickness was set 3.0 mm to get the lower oxygen level at the same Q/Q_0.

In comparison, the data at 1.5 mm in thickness and Q/Q_0 = 500% was shown in Fig. 6. Its oxygen level was achieved below 2 mass%O. This implies that many slim baskets can lie in parallel as the cathode to get a high productivity per charge and a fast reducing rate.

3.3 Dehydration prior to electrolysis

Relatively high oxygen level was obtained even in a slim basket as shown in the previous section. Because a large quantity of electric charge such as $Q/Q_0 = 200\%$ was applied, much lower oxygen level should be achieved if the efficiency

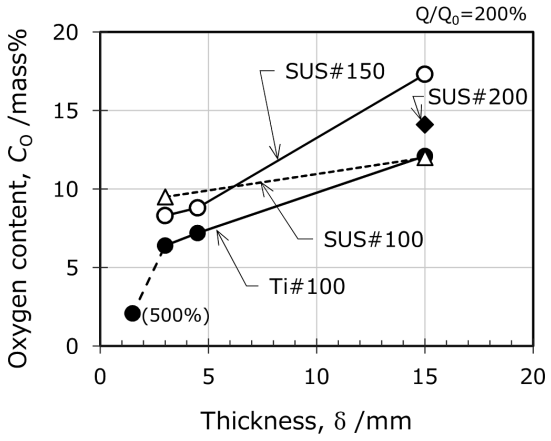

Fig. 6 Residual oxygen in the cathodic powder.

is enough high.

One of the reasons for this low efficiency is the existence of water in $CaCl_2$. Because $CaTiO_3$ and CaO were calcined at high temperatures, impurity water in hygroscopic $CaCl_2$ is the source of water in the system. In order to decompose monohydrate of $CaCl_2$, dehydration above 543 K, favorably above 573 K, is needed. Quick handling of salt at room temperature is off course needed, and the dehydration at the elevated temperature as high as 873 K will be effective in the same vessel for reaction.

Figure 7 shows various related parameters for dehydration. The result of dehydration effect was evaluated as the residual oxygen in the sample after the electrolysis. When the larger amount of water remained in the system, the higher current is needed for water decomposition and the current efficiency becomes worse. Evacuation is one of the easy methods to remove water, and it was applied for $CaCl_2$-CaO melt. At temperatures below melting, such as at 873 K, water was not effectively removed.

A small dependency of CaO concentration on the residual amount of oxygen could be seen in Fig. 7. At the higher concentration of CaO, the larger amount of Ca is generated and the stable current during the electrolysis becomes larger. Then the same quantity of electric charge was achieved within the shorter time. However, a sufficient diffusion did not occur and deteriorated the quality of sample concerning the residual amount of oxygen.

Dehydration above melting of $CaCl_2$ (1045 K) was more effective to shorten the dehydration period, and to improve the attainable oxygen level. Water electrolysis using two carbon electrodes in vacuum were very efficient and shortened the dehydration time than the simple vacuum dehydration, as shown in Fig. 7.

3.4 Optimization of CaO concentration

Because the starting material $CaTiO_3$ contains CaO in the crystalline structure, CaO is automatically fed to the $CaCl_2$ melt during the electrolysis. $CaCl_2$-0.5 mol%CaO has been often used for TiO_2 reduction[9,21–23], but the CaO addition was found not necessary for $CaTiO_3$ except for the initial stage of electrolysis. Previous studies reported smooth electrolysis when 0.5 mol%CaO was added, but the effects of CaO were not well studied[30,34].

Figure 8 shows the oxygen concentration analysis of the samples after the electrolysis of Q/Q_0 = 200 or 600%. The residual oxygen concentration was the lowest at the CaO concentration near 0.2 mol%CaO. When CaO concentration was higher than 0.5 mol%, the oxygen concentration in the obtained powder was as high as 6–8 mass%O, as shown in Fig. 7. Note that the CaO concentration given in Fig. 8 was estimated as the sum of the initial amount of CaO and the amount of CaO supplied from the reduced $CaTiO_3$. The supplied amount of CaO from $CaTiO_3$ becomes dominant at the optimal concentration range of CaO in $CaCl_2$ bulk, and the initial charge of $CaTiO_3$ was less than 2.0 g to examine the dilute region. The data without any addition of CaO in $CaCl_2$ was well consistent with the data with a small addition of CaO, as shown in Fig. 8. Therefore, the specification of origin of CaO was not needed.

When the larger quantity of electric charge was given; Q/Q_0 = 600%, the residual amount of oxygen becomes smaller than those at Q/Q_0 = 200%.

These results were obtained by using $CaTiO_3$ purchased from the producer #A. When $CaTiO_3$ purchased from the producer #F was taken at Q/Q_0 = 600%, the lowest oxygen concentration in this work was achieved as 4200 mass ppmO. The experimental difference was the particle size as mentioned later, but some other parameters were also modified: the cathode was rapidly cooled in extra-high purity argon (Ex-Ar, less than 10 vol ppm oxygen) gas. This excellent value is comparable with the industrial purity. Hereafter the reason why such an excellent data was obtained is studied.

3.5 Particle size

It is certain that the size of oxide particles affects the obtained oxygen level. In case of oxide pellet with a few tens mm, it would take a longer time for oxygen to diffuse from the inner part to the external surface, however, it does not take so long time in a powder form at the calciothermic reduction. The effect of particle size of oxide was checked by using a few commercial $CaTiO_3$ powder.

The particle size distributions of four producers were measured as shown in Fig. 9. Fairly sharp distribution is found in #S, and very fine particles are included in #A. The distribution of #F extended to a large size. The powder #F was milled in agate mortar, and the distribution of pulverized powder was measured as "#F crushed" in Fig. 9. The median size D_{50} were

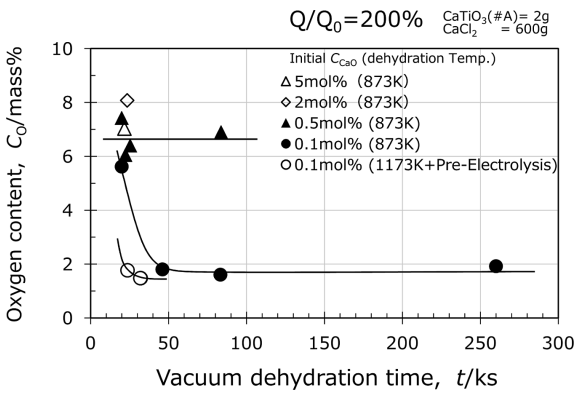

Fig. 7 Residual oxygen in the obtained samples after the electrolysis as a function of dehydration time, temperature and CaO content.

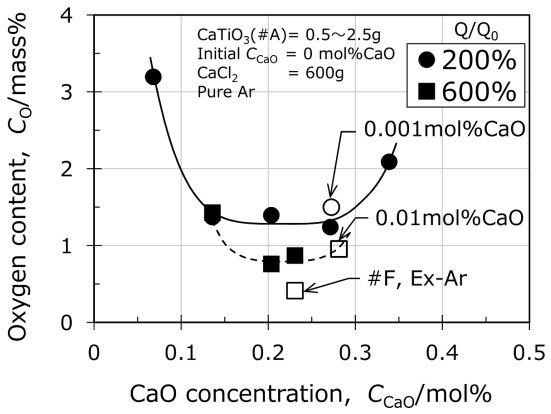

Fig. 8 CaO concentration dependency of oxygen concentration in the obtained sample after the electrolysis at Q/Q_0 = 200 and 600%.

evaluated as inserted in Fig. 9. By milling the powder #F, the volume fraction of smaller particles increased and D_{50} of #F (5.8 μm) was halved to 3.7 μm. XRD analysis showed that the powder #K contained a small amount of TiO_2 and it was not used hereafter.

Here CaO was not added to the initial charge of $CaCl_2$, and the initial concentration of CaO in the molten salt was set zero. 1.7 g of $CaTiO_3$ powder in the cathodic basket was inserted in 600 g melt. CaO concentration after the electrolysis is estimated as 0.23 mol%CaO in the melt, assuming both the complete reduction to metal Ti and the complete dissolution of residual CaO. All the samples (#A, #F, #F crashed, #S) were cooled in the extra-high purity argon (Ex-Ar).

As shown in Fig. 10, the oxygen concentration after electrolysis ($Q/Q_0 = 600\%$) decreased as the initial oxide particle size was larger. Because the total amount of obtained metallic powder was small, the size distribution of metallic powder could not be analyzed. However, it is noted that the pulverized and reduced powder (#F crashed) contained a larger amount of oxygen than that in the sample reduced simply from #F. Because the finer powder of the oxide contained very fine particles in addition to the larger grains, the surface contamination of these fine metallic Ti particles may attribute to the higher oxygen concentration. The surface area of metallic powder should be considered in their fabrication. The degree of sintering during the electrolysis is a sensitive parameter in seeking for lower oxygen concentration. The control of size distribution may be one of the good approaches to reduce the apparent oxygen content in the powder.

Figure 11 shows the SEM image of the reduced powder #F. The smooth surface without asperity extends over the sample, which represents a good sintering behavior. No twin structure was found, which often indicates oxygen concentration higher than 1 mass%. The size of conglomerated particles was larger than 10 μm.

3.6 Oxidation in CO_2 and CO gas

Before solidification of molten salt, the electrodes were pulled up in order to remove the solidified salt easily. During electrolysis, CO_2 and CO gas were emitted from the bath to the vessel and exhausted out from the outlet using a slow feeding rate of Ar gas at the top of vessel. Therefore, there is a risk to oxidize the reduced sample during cooling in the environment of CO_2 and CO gas.

The oxidation behavior of Ti in these gases was not clarified in the literatures. The oxidation of titanium powder (Osaka Titanium technologies Co. Ltd., Ti sponge produced by Kroll method was pulverized by hydrate-dedydrate process in hydrogen gas) was experimentally tested without electrolysis. The Ti powder (<#300 mesh) was filled in an alumina crucible (33 mm in inside diameter) and heated at 1173 K for 7.2 ks. The atmosphere surrounding the Ti powder was switched from Ar gas to the gas mixture of CO_2 and CO gas. After cooling in the applied gas flow, the sample was recovered from the crucible, as shown in Fig. 12. The upper surface was black with white spots, while the lower part was gray.

The phases were identified by XRD measurements as TiC + Ti_3O, and Ti + TiC, at the upper and lower parts, respectively, in the crucible. It is noted that TiC forms a complete solid solution (NaCl-type) with TiO, and it is difficult to identify it as TiC and TiO separately. Ti_3O is a highly oxygen-containing phase derived from α-Ti at 1173 K[5]. Although the stacking of Ti powder was not dense, the upper part reacted well with CO_2 gas to form TiC or Ti(C,O) solid solution,

$$\mathrm{Ti} + \mathrm{CO_2(g)} = \mathrm{Ti(C,O)}_{1-y} + \mathrm{Ti}_x\mathrm{O} + y\mathrm{CO(g)} \qquad (11)$$

$$\mathrm{Ti} + \mathrm{CO(g)} = \mathrm{Ti(C,O)} + z\mathrm{Ti_3O} \qquad (12)$$

and the lower part did not react well with the gas and it remained as metallic Ti.

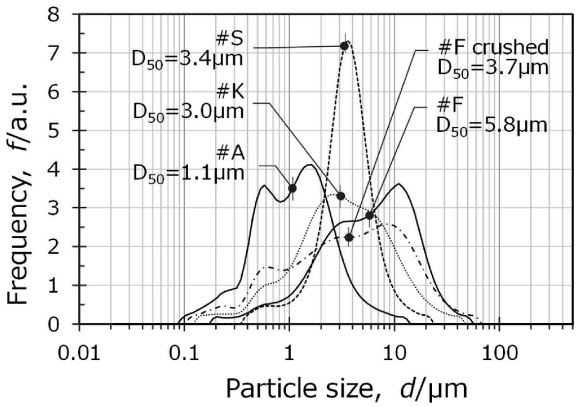

Fig. 9 Particle size distribution of $CaTiO_3$ powders from four producers, #A, #K, #S and #F.

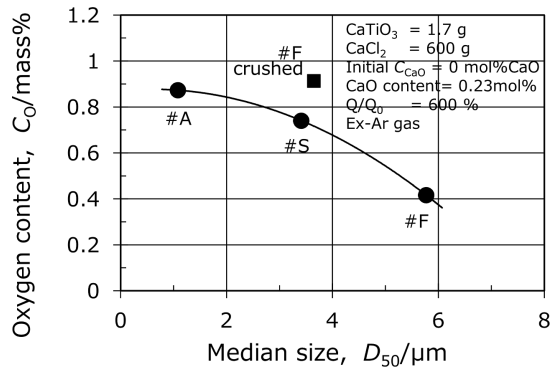

Fig. 10 Particle size dependency of oxygen concentration in the obtained sample after the electrolysis at $Q/Q_0 = 600\%$.

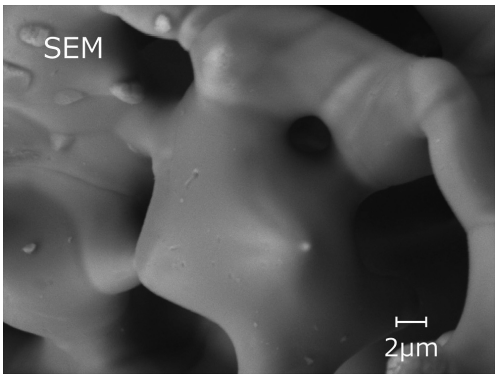

Fig. 11 SEM image of the reduced sample (#F), to which $Q/Q_0 = 600\%$ was given. The sample was cooled in EX-Ar.

The oxygen concentration at the upper part was analyzed when the sample was heated either in the pure Ar gas, pure CO_2 gas, pure CO gas or their gas mixture. The initial concentration of pure Ti powder was 0.273 mass%O, and increased to 0.63 mass%O even in pure Ar gas (purity 99.997%).

Figure 13 shows the oxidation behavior under various gases. The oxygen content increased as the concentrations of CO_2 and CO gas increased. Both CO_2 and CO gas in the vessel were not neutral for maintaining metallic titanium, and they oxidized the titanium powder significantly.

The reactivity of Ti with CO_2 and CO gas can be predicted from the thermodynamic data[6], but the increment of oxygen content became clear. If the exhaust gas during the electrolysis contains a few vol%CO_2 in Ar-CO_2 gas mixture, it is natural that the obtained Ti powder after the electrolysis was easily oxidized to several mass%O. If the exhaust gas is so reactive for oxidizing the obtained titanium, the Ti metal after the electrolysis should be kept far from this oxidizing environment.

3.7 Cooling condition

Some attempts in cooling were tried so that the samples might be isolated from the exhaust gas. Figure 14(a) shows the setup during electrolysis. After stopping the current between two electrodes, they were pulled up as shown in Fig. 14(b). The vessel was evacuated at the pressure of 7 Pa, and the cathodic basket was cooled rapidly in the cooling tube equipped at the upper part of vessel. The coolant water was circulated at 293 K through heat exchanger. In vacuum the cooling rate might be slow due to thermal isolation. Instead of vacuum as shown in Fig. 14 (c), 1 atm of pure Ar gas (99.997%) or extra-high purity Ar (Ex-Ar, 99.9995%) was introduced into the vessel, and the cathode basket was also cooled at the upper part. In comparison, the basket remained in the bath during slow cooling in Ex-Ar gas, as shown in Fig. 14 (d). The cooling rate was $1/60\ \mathrm{Ks}^{-1}$ by arriving at 573 K. The samples were picked up by dissolving in hot water.

The obtained phases and oxygen concentration were listed in Table 1. As mentioned above, the oxygen concentration of 0.42 mass% could be marked when the cathodic basket was rapidly cooled in EX-Ar. The continuous evacuation or Ar gas filling with normal-high purity was not sufficient to protect the samples from high-temperature corrosion due to CO/CO_2 gas.

Titanium is well known as the getter material to maintain a high vacuum because the leaked oxygen and nitrogen react with titanium and because they are absorbed in Ti. Even if CO and CO_2 gas react mildly with titanium, the carbon and oxygen decomposed from these gases are absorbed in the titanium metal. Because the reduced Ti powder is so fine, its surface will be easily oxidized during cooling. Evacuation from the vessel should be challenged to much lower pressure, and highly purified Ar gas circulation might be one of solutions. Coarsening of obtained Ti powder and residual salt on the particle surface may give some protective properties against high temperature corrosion.

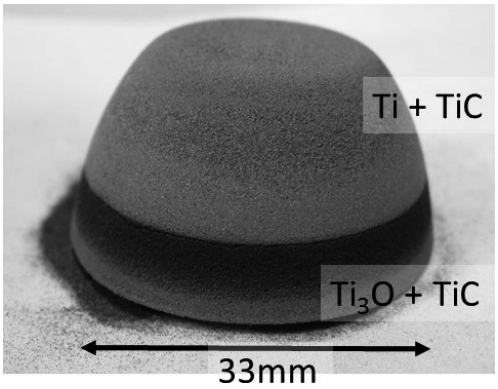

Fig. 12 Photo of the Ti powder after picked up from the cup-type alumina crucible. The powder was heated in CO_2 gas at 1173 K for 7.2 ks, and the bottom side of slightly sintered powder was reversed for photography.

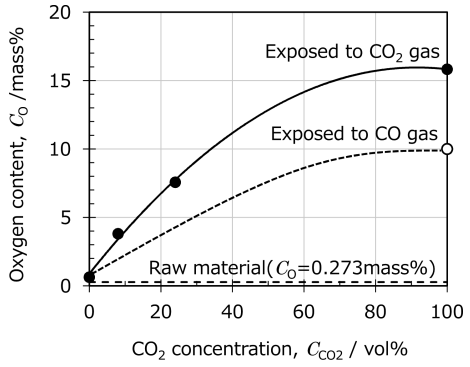

Fig. 13 Oxidation behavior of Ti powder under various gases.

4. Conclusions

Basic understanding on calciothermic reduction is presented using the molten salt electrolysis of CaO in $CaCl_2$ melt. Impurity phase $CaTiO_3$ existing on the way from the oxide TiO_2 to metallic Ti might have disturbed healthy operation. This work studied the reduction of $CaTiO_3$, as a part of long scheme as shown in Fig. 2. The strategy to reduce $CaTiO_3$ bases on abundant existence of $TiFeO_3$, and an intermediate product $CaTiO_3$ was reduced as the starting oxide in the molten salt electrolysis. Inhomogeneous growth of metallic part in the metallic basket is related with buoyancy of Ca and insufficient dehydration, as shown in Fig. 5. Slim basket may give a low and homogeneous oxygen concentration. The dehydration from $CaCl_2$ at the solid state was weak, and it is better to remove water from the liquid state by long evacuation. Optimal CaO concentration was 0.2 mol%CaO to achieve 0.42 mass%O, as low as the industrial level. To pursue to lower oxygen level, the possible oxidation due to CO/CO_2 gas during cooling is also avoided. ZrO_2 membrane or oxygen absorbing anode may be able to separate the emitted gas[38]. The atmospheric impurity in vessel will contribute the oxygen level, which may be caused also in industrial scale. Thus this study analyzed some possible reduction mechanisms coming from $CaTiO_3$, which may assist to operate the reduction from TiO_2.

Acknowledgments

The authors thank Dr. Hideki Fujii at Nippon Steel and Su-

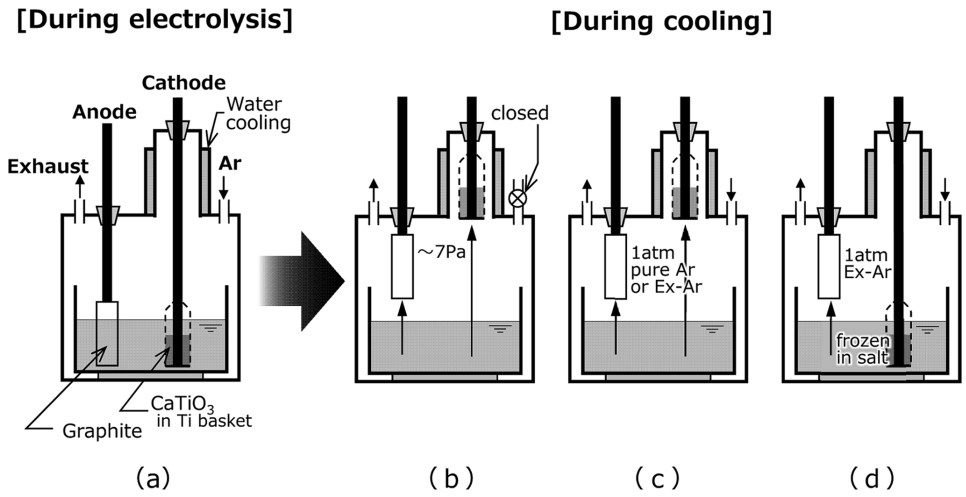

Fig. 14 (a) experimental setup during electrolysis, (b) cooling in vacuum where the cathode was cooled at the upper part, (c) cooling in pure Ar or Ex-Ar, and (d) cooling in the frozen salt.

Table 1 Phase identification and analyzed oxygen concentration in the cooled samples. 1.7 g of $CaTiO_3$ (#F) was reduced in pure $CaCl_2$ without any addition of CaO.

	Cooling method illustrated in Fig. 13				
	(b)	(c)		(d)	
Run number	#93	#92	#80	#84	#102
Supplied charge, Q/Q_0	600.1%	620.8%	627.8%	610.1%	600.0%
Cooling atmosphere	In vacuum, About 7 Pa	Pure Ar, 1 atm	Extra-pure Ar, 1 atm		In vacuum, About 3 Pa
Cooling position	In the cooling tube placed on the lid of stainless steel vessel			Frozen with the salt	
Phase identified by XRD and its volume fraction	α-Ti (94%), Ti_3O (5%) TiO (1%)	α-Ti (100%)	α-Ti (100%)	α-Ti (100%)	α-Ti (99%), TiO (1%)
Oxygen concentration, C_O/mass%	1.51	0.76	0.42	1.19	2.84

mitomo Metal Co. Ltd. (Presently at Toho Titanium Co. Ltd.) for his keen comments and discussions during this work. They also thank Ms Mika Kitamura and Ms Mariko Takahashi for their sincere assistance in experiments. This study was financially supported by the Grants-in-Aid for Scientific Research (No. 25289267), by Advanced Low Carbon Technology Research and Development Program (ALCA), Japan Science and Technology Agency (JST), and by New Energy and Industrial Technology Development Organization (NEDO) under the "Innovative Structural Materials Project (Innovative Structural Materials Association (ISMA), Future Pioneering Projects).

REFERENCES

1) G.Z. Chen, D.J. Fray and T.W. Farthing: Nature **407** (2000) 361–364.
2) C. Schwandt and D.J. Fray: Electrochim. Acta **51** (2005) 66–76.
3) C. Schwandt, G.T.L. Alexander and D.J. Fray: Electrochim. Acta **54** (2009) 3819–3829.
4) C. Schwandt, G.R. Daughty and D.J. Fray: Key Eng. Mater. **436** (2010) 13–25.
5) H. Okamoto, "Desk Handbook Phase Diagrams for Binary Alloys," ASM International, Materials Park, OH, (2000).
6) A. Roine, HSC Chemistry, ver.8.0.8, Outotec Oyj, Pori, Finland, (2014).
7) K. Ono, R.O. Suzuki and J.O.M. Mem: J. Miner. Met. Mater. Soc. **54** (2002) 59–61.
8) R.O. Suzuki and S. Inoue: Metall. Mater. Trans., B **34** (2003) 277–285.
9) R.O. Suzuki, K. Teranuma and K. Ono: Metall. Mater. Trans., B **34** (2003) 287–295.
10) B. Neumann, C. Kröger and H. Jüttner: Z. Elektrochem. **41** (1959) 725–736.
11) D.A. Wenz, I. Johnson and R.D. Wolson: J. Chem. Eng. Data **14** (1969) 250–252.
12) G.S. Perry and L.G. MacDonald: J. Nucl. Mater. **130** (1985) 234–241.
13) D.T. Peterson and J.A. Hinkebein: J. Phys. Chem. **63** (1959) 1360–1363.
14) R.A. Sharma: J. Phys. Chem. **74** (1970) 3896–3900.
15) V. Dosaj, C. Aksaranan and D.R. Morris: J. Chem. Soc., Faraday Trans. I **71** (1975) 1083–1098.
16) H. Fischbach: Steel Res. **56** (1985) 365–68.
17) L.-I. Staffansson and S. Du: Scand. J. Metall. **21** (1992) 165–171.
18) A.I. Zaitsev and B.M. Mogutnov: Metall. Mater. Trans., B **32** (2001) 305–311.
19) T. Takenaka, T. Morishige and M. Umehara, Molten Salts Chemistry and Technology, ed. M. Gaune-Escard and G. M. Haarberg, John Wiley & Sons, Chichester, UK, (2014) pp.143–148.
20) T. Takenaka, K. Shigeta, H. Masuhama and K. Kubota: ECS Trans. **16** (2009) 441–448.
21) R.O. Suzuki and S. Fukui: Mater. Trans. **45** (2004) 1665–1671.

22) R.O. Suzuki: J. Phys. Chem. Solids **66** (2005) 461–465.
23) K. Kobayashi, Y. Oka and R.O. Suzuki: Mater. Trans. **50** (2009) 2704–2708.
24) J. Mohanty, K.G. Mishra, R.K. Paramguru and B.K. Mishra: Metall. Mater. Trans., B **43** (2012) 513–518.
25) B. Bhagat, D. Dye, S.L. Raghunathan, R.J. alling, D. Inman, B.K. Jackson, K.K. Rao and R.J. Dashwood: Acta Mater. **58** (2010) 5057–5062.
26) M.P. Rogge, J.H. Caldwell, D.R. Ingram, C.E. Green, M.J. Geselbracht and T. Siegrist: J. Sold State Chem. **141** (1998) 338–342.
27) T.H. Okabe, R.O. Suzuki, T. Oishi and K. Ono: Mater. Trans., JIM **32** (1991) 485–488.
28) T.H. Okabe, R.O. Suzuki, T. Oishi and K. Ono: Tetsu-to-Hagane **77** (1991) 93–99.
29) K.T. Jacob and S.T. Gupta: Bull. Mater. Sci. **32** (2009) 611–616.
30) N. Kobayashi, K. Kobayashi, T. Kikuchi, R.O. Suzuki, Proc. 12th World Conf. on Titanium, ed. by L. Zhou, H. Chang, Y. Lu, D. Xu, Science Press, Beijing, China, (2011) vol.I, pp.84–86.
31) R.C. DeVries, R. Roy and E.F. Osborn: J. Phys. Chem. **58** (1954) 1069–1073.
32) H.E. Tulgar: Istanbul Tek. Univ. Bul. **29** (1976) 111–129.
33) K.T. Jacob and K.P. Abraham: J. Chem. Thermodyn. **41** (2009) 816–820.
34) K. Jiang, X.H. Hu, M. Ma, D.H. Wang, G.H. Qiu, X.B. Jin and G.Z. Chen: Angw. Chem. Int. Ed. **45** (2006) 428–432.
35) X.G. Lu, X.L. Zou, C.H. Li, Q.D. Zhong, W.Z. Ding and Z.F. Zhou: Metall. Mater. Trans., B **43** (2012) 503–512.
36) M. Panigrahi, E. Shibata, A. Iizuka and T. Nakamura: Electrochim. Acta **93** (2013) 143–151.
37) C.-C. Qi, Y.-X. Hua, K.-H. Chen, Y.-F. Jie, Z.-R. Zhou, J.-J. Ru, L. Xiong and K. Gong: J. Miner. Met. Mater. Soc. **68** (2016) 668–674 (JOM).
38) N. Asahara, M. Yoshida, Y.Matsuoka and R.O. Suzuki, Molten Salt XIV, ed. by R.A. Mantz, P.C. Trulove, H.C. De Long, C.R. Stafford, M. Hagiwara and D.A. Costa, The Electrochemical Society, Penningston, NJ, USA, (2006) 1063–1070.